Research Article

Lothar Noethe*, Pietro Schipani, Ronald Holzlöhner and Andrew Rakich

A method for the use of ellipticities and spot diameters for the measurement of aberrations in wide-field telescopes

Abstract: In wide-field survey telescopes, the patterns of spot sizes and ellipticities can be used to determine wavefront aberrations generated by the telescope. The calculation of spot sizes and ellipticities generated by telescope aberrations is most conveniently done if the aberrations are expressed in terms of Zernike-type polynomials whose derivatives are orthonormal. The field dependence of the spot sizes and ellipticities generated by the telescope can conveniently be expressed by low-order Zernike polynomials. Because the exposure times in astronomical survey work are typically rather short, this information may be used for a quasi-closed loop control of the telescope optics. The ability to accurately subtract ellipticities generated by telescope errors could also be useful for observations such as gravitational lensing surveys.

Keywords: active optics; ellipticities; telescope aberrations; wide-field telescopes.

DOI 10.1515/aot-2014-0024
Received March 21, 2014; accepted May 9, 2014

1 Introduction

The focal plane of a wide-field telescope is often nearly completely covered by the detector, usually an array of CCD chips. This precludes the option to pick up the light of sufficiently bright stars for wavefront sensors in arbitrary locations in the field during astronomical exposures. Instead, the image quality is often measured using wavefront sensors at the edge of the field outside the science field. One option is to use additional, axially displaced chips in this area. The telescope aberrations are then deduced from characteristics of defocused star images [1].

However, information about the telescope aberrations may also be obtained by analyzing the variations of the diameters and ellipticities of the images of point sources across the field. The large amount of data given by the large number of stars in the field reduces the noise that is due to the measurements of the characteristics of individual spots. Together with the wavefront information derived from a wavefront sensor at the edge of the field, the image quality of a wide-field telescope can then be monitored and, possibly, also be controlled in closed loop between the rather short exposures typical of astronomical survey work. This task should be simplified by the fact that, most of the time, the pointing and, therefore, also the optical aberrations generated by the telescope do not change significantly between exposures.

The effect of telescope aberrations on spot sizes and ellipticities has been studied by several authors, often in the context of weak lensing investigations [2–8]. All these papers describe methods and attempts to extract telescope errors from the spot characteristics across the field. In addition, they also contain several references to earlier work in this field.

This paper deals primarily with two issues. First, a classification of telescope aberrations that affect the spot sizes and generate ellipticities is more easily done in terms of Zernike-type polynomials, whose derivatives are orthonormal across the pupil, than in terms of the standard Zernike polynomials. The use of these polynomials, which will be called slope Zernike polynomials, also simplifies the calculation of the spot parameters.

Second, all spot size and ellipticity patterns across the field that are generated by telescope errors can readily be

***Corresponding author: Lothar Noethe,** ESO, Karl-Schwarzschild Strasse 2, Garching 85748, Germany,
e-mail: lnoethe@eso.org
Pietro Schipani: INAF – Osservatorio Astronomico di Capodimonte, Napoli, Italy
Ronald Holzlöhner and Andrew Rakich: European Southern Observatory, Garching, Germany

expanded in terms of standard Zernike polynomials. Such information can reduce and constrain the set of functions fitted to the measured spot sizes and ellipticities.

Section 2 describes the definition of spot sizes and ellipticities, how they are, for a given field location, related to the derivatives of slope Zernike polynomials, and how their dependence on the field locations can be characterized by Zernike polynomials. Section 3 describes the aberrations that are expected in wide-field telescopes and that affect the spot sizes and ellipticities. Section 4 describes the expected field patterns of spot sizes and ellipticities and shows that all of them can be well represented by Zernike polynomials. Finally, Section 5 describes possible procedures to extract telescope errors from the field patterns of spot sizes and ellipticities.

2 Relationship between ellipticities and wavefront aberrations

2.1 Definition of spots sizes and ellipticities

For ground-based telescopes, two factors preclude diffraction-limited imaging: atmospheric turbulence and telescope errors. For exposures of at least a few seconds, the aberrations generated by the atmosphere lead to approximately circular seeing discs with root mean square (rms) values of the order of 0.5 arcsec under average conditions.

In large telescopes, the size of the seeing disc is much larger than the size of the Airy disc created under diffraction-limited conditions. Therefore, the additional effects due to telescope aberrations are best described by geometrical rather than diffraction optics, or, in other words, by wavefront slope errors rather than wavefront errors. The shape of an image of a point source can then be modeled as the sum of the point spread functions generated by the atmosphere on the one hand and the telescope errors on the other hand.

Let σ_l and σ_s denote the measured rms values along the long and short axes of a possibly elliptical spot, and α_m the measured orientation of the ellipse, defined as the angle of the long axis of the ellipse with the x-axis. These are the only measurable spot parameters that will be used in this study. A common definition η of the modulus of a relative ellipticity is:

$$\eta=\frac{\sigma_l}{\sigma_s}-1. \tag{1}$$

For several reasons given below, a different definition of the modulus ϵ_m of the measured ellipticities is used in this study:

$$\epsilon_m=\sigma_l^2-\sigma_s^2. \tag{2}$$

A problem, for both definitions, is the ambiguity of the orientation, because the true, measured angles α_m and $\alpha_m+\pi$ are equivalent. This ambiguity can be resolved by defining the angle of the ellipticity as $2\alpha_m$ rather than α_m. Together with the modulus $\sigma_l^2-\sigma_s^2$, this defines a unique ellipticity vector $\vec{\epsilon}_m$.

The next task is to relate this ellipticity vector $\vec{\epsilon}_m$ to calculable second moments of point spread functions generated by aberrations $w(r, \varphi)$, where r is the normalized radial and φ the azimuth pupil coordinate. Let r_p be the half-diameter of the pupil and $u, v \in \{x, y\}$, where x and y are normalized coordinates. The second moments μ_{uv} of point spread functions due to wavefront aberrations $w(r, \varphi)$ without tilt components are then given by:

$$\mu_{uv}=\frac{1}{\pi r_p^2}\int_0^{2\pi} d\varphi \int_0^1 r dr \left[\frac{\partial}{\partial u}(w(r,\varphi))\right]\cdot\left[\frac{\partial}{\partial v}(w(r,\varphi))\right]. \tag{3}$$

The mean square d_{spot}^2 of the spot diameter is defined by:

$$d_{spot}^2=\mu_{xx}+\mu_{yy}. \tag{4}$$

The ellipticity ϵ and the angle α of its long axis with the x-axis are defined by:

$$\epsilon=\sqrt{(\mu_{xx}-\mu_{yy})^2+4\mu_{xy}^2}, \tag{5}$$

$$\alpha=\frac{1}{2}\arctan\frac{2\mu_{xy}}{\mu_{xx}-\mu_{yy}}. \tag{6}$$

This expression for ϵ has the dimension rad^2.

The definition can be compared with the definition of the polarization using the Stokes parameters. The first term under the square root in Eq. (5) is equivalent to the square of the Stokes Parameter S_1, whereas the second term is equivalent to $S_2^2+S_3^2$.

A similar definition of the ellipticity is used in [4], where the expression in Eq. (5) has been normalized by a division by the square of the spot size. Because the latter is equivalent to the Stokes parameter S_0, the definition of the ellipticity in [4] is equivalent to the usual definition of the polarization.

In this paper, expressions for ϵ and α will be calculated analytically. By definition, always the positive square root will be taken in Eq. (5). However, because the expressions

will be analytical functions of the field coordinates, often including trigonometric functions of the field angle, ϵ may still be positive or negative.

The angle α derived from Eq. (6) is ambiguous. Because of the ambiguity of the arctan function, the two angles α and $\alpha-\pi/2$ could both be used to characterize the orientation.

The true angle will be defined as the principal value of the arctan function if ϵ is positive and as the principle value plus 90° if ϵ is negative. Therefore, a change of the sign of ϵ rotates the true orientation of the ellipticity by 90°.

In line with the definition of the measured ellipticity vector $\vec{\epsilon}_m$, where the angle α_m has been doubled, a calculated ellipticity vector $\vec{\epsilon}$ is defined with the double angle 2α. Its x- and y-components are defined by:

$$\epsilon_x=\epsilon\cos 2\alpha, \tag{7}$$

$$\epsilon_y=\epsilon\sin 2\alpha. \tag{8}$$

Therefore, a change of the sign of ϵ rotates the ellipticity vector $\vec{\epsilon}$ by 180°. This definition of $\vec{\epsilon}$, calculated from the moments, is consistent with the definition of the components of the ellipticity vector $\vec{\epsilon}_m$ derived from the measured parameters $\sigma_l^2-\sigma_s^2$ and the unambiguous angle $2\alpha_m$:

$$\epsilon_x=\epsilon\cos 2\alpha=(\sigma_l^2-\sigma_s^2)\cos 2\alpha_m, \tag{9}$$

$$\epsilon_y=\epsilon\sin 2\alpha=(\sigma_l^2-\sigma_s^2)\sin 2\alpha_m. \tag{10}$$

The definition of the ellipticity as a difference between σ_l^2 and σ_s^2 has another major advantage. As long as the point spread function of the seeing disc is symmetrical, the contributions of the seeing to σ_l^2 or σ_s^2 are independent of the contributions from other aberrations [9]. The rms σ_{seeing} due to seeing is then an independent and identical term in each of the quadratic sums leading to σ_l^2 and σ_s^2. Therefore, the definition of the ellipticity as the difference between σ_l^2 and σ_s^2 is independent of the seeing. However, this statement should be tested empirically.

The visual impression of the ellipticity of a spot is better described by Eq. (1). Usually, the spot sizes are dominated by the seeing rather than by the telescope aberrations. Assuming that $\sigma_l^2-\sigma_s^2\ll\sigma_{seeing}^2$, η is approximately given by:

$$\eta\approx\frac{1}{2}\frac{\sigma_l^2-\sigma_s^2}{\sigma_{seeing}^2}. \tag{11}$$

Therefore, for small ellipticities, also the visual impression of the ellipticity is proportional to $\sigma_l^2-\sigma_s^2$.

The lower limit for detecting ellipticities is $\eta\approx7\times10^{-5}$ (see Section 4.8.1). Assuming a seeing with $\sigma_{seeing}\approx0.5$ arcsec, a corresponding ellipticity ϵ_0, expressed in terms of the difference between σ_l^2 and σ_s^2, is defined as:

$$\epsilon_0=(\sigma_l^2-\sigma_s^2)_0\approx8.2\cdot10^{-10}\ \text{mrad}^2\approx(0.006'')^2. \tag{12}$$

This ellipticity ϵ_0 could be used as a reference. However, weak lensing surveys require maximum noise levels of $\eta\approx10^{-3}$ [4], which is approximately equivalent to $14\epsilon_0$. Therefore, a reference ellipticity $\epsilon_{WL}\approx14\epsilon_0\approx1.2\times10^{-14}$ will be used for comparisons of values for ϵ occurring in real telescopes with the requirements for weak lensing surveys.

The measured mean square $d_{spot,m}^2$ of the spot size is defined as:

$$d_{spot,m}^2=\frac{1}{2}(\sigma_l^2+\sigma_s^2), \tag{13}$$

which does strongly depend on the seeing.

In cases where the seeing is the dominant contributor to the degraded image quality, the seeing can be removed by defining the variations of the spot size due to the telescope errors as:

$$d_{tel,m}^2=\frac{1}{2}(\sigma_l^2+\sigma_s^2-2\sigma_{s,min}^2). \tag{14}$$

However, although this definition certainly removes the largely constant contribution due to the seeing, it also removes some contributions from telescope errors that are constant across the field.

2.2 Ellipticities generated by single or sums of two Zernike polynomials

The standard orthonormalized Zernike polynomials are denoted by $Z_{m,j,a}(r,\varphi)$, where m is the rotational symmetry, j is the order within the rotational symmetry, starting with $j=1$, and $a\in\{c, s\}$, where the suffixes c and s stand for the cosine and sine components, respectively. The radial parts $\tilde{R}_{m,j}(r)$ of the standard Zernike polynomials are defined by:

$$Z_{m,j,c}(r,\varphi)=\tilde{R}_{m,j}(r)\cos m\varphi, \tag{15}$$

$$Z_{m,j,s}(r,\varphi)=\tilde{R}_{m,j}(r)\sin m\varphi. \tag{16}$$

The abbreviated notation $Z_{m,j}(r,\varphi)$ will stand for either $Z_{m,j,c}(r,\varphi)$ or $Z_{m,j,s}(r,\varphi)$. For example, the Zernike polynomial corresponding to defocus is denoted by $Z_{0,2}(r,\varphi)$. Other common names and notations for some low-order

Zernike polynomials $Z_{m,j}(r, \varphi)$ are given in Table 4 in Appendix 7.1.

However, ellipticities are parameters of the shape of point spread functions. Therefore, for the description of the wavefront errors generating the point spread functions, it should be appropriate to use Zernike-type polynomials, whose derivatives are orthogonal over the unit circle [10, 11]. These functions, in this paper called slope Zernike polynomials, will be denoted by $S_{m,j,\mathrm{a}}(r, \varphi)$.

The radial parts $\tilde{B}_{m,j}(r)$ of the polynomials $S_{m,j,\mathrm{a}}(r,\varphi)$ are defined by:

$$S_{m,j,\mathrm{c}}(r,\varphi)=\tilde{B}_{m,j}(r)\cos m\varphi, \tag{17}$$

$$S_{m,j,\mathrm{s}}(r,\varphi)=\tilde{B}_{m,j}(r)\sin m\varphi. \tag{18}$$

The abbreviated notation $S_{m,j}(r, \varphi)$ will stand for either $S_{m,j,\mathrm{c}}(r, \varphi)$ or $S_{m,j,\mathrm{s}}(r, \varphi)$. Formulae for the conversion of the Zernike polynomials to slope Zernike polynomials are given in Appendix 7.2.

In survey telescopes with large fields, the central obstructions are rather large. A description of the pupil aberrations would then profit from the use of slope Zernike polynomials that are orthogonal over an annular pupil. However, for simplicity, all examples given in this paper are using slope Zernike polynomials for a full circular pupil.

If the letter C at the bottom of the integral symbol denotes the integration over a circular, possibly annular pupil with an outer normalized radius r=1, the slope Zernike polynomials are normalized such that:

$$\begin{aligned}&\frac{1}{\pi r_\mathrm{p}^2}\int_C\left[\frac{\partial}{\partial x}S_{m_1,j_1,\mathrm{a}}(r,\varphi),\frac{\partial}{\partial y}S_{m_1,j_1,\mathrm{a}}(r,\varphi)\right]\cdot\\&\left[\frac{\partial}{\partial x}S_{m_2,j_2,\mathrm{b}}(r,\varphi),\frac{\partial}{\partial y}S_{m_2,j_2,\mathrm{b}}(r,\varphi)\right]\\&=\frac{1}{r_\mathrm{p}^2}\delta_{m_1,m_2}\delta_{j_1,j_2}\delta_{\mathrm{a,b}},\end{aligned} \tag{19}$$

where δ denotes the Kronecker delta.

For a coefficient c of $S_{m,j,\mathrm{a}}(r, \varphi)$, the root mean square of the point spread function measured in radians is c/r_p. Ellipticities for c/r_p=1 will be denoted by ϵ_n.

The derivative of a slope Zernike polynomial $S_{m,j,\mathrm{a}}(r, \varphi)$ with respect to x and y can be expressed as a single Zernike polynomial $Z_{1,j-1,\mathrm{a}}(r, \varphi)$ for m=0 or as a sum of two Zernike polynomials $Z_{m-1,j,\mathrm{b}}(r, \varphi)$ and $Z_{m+1,j-1,\mathrm{b}}(r, \varphi)$ for m>0, with a, b∈{c, s}. Explicit formulae are given in Eqs. (66) to (71) in Appendix 7.3.

A wavefront error w(r, φ) will be described as a sum of slope Zernike polynomials $S_{m,j,\mathrm{a}}(r, \varphi)$. Therefore, the second moments defined in Eq. (3) can contain terms with two identical or two different slope Zernike polynomials:

$$\begin{aligned}\mu_{m_1j_1m_2j_2\mathrm{ab},uv}=\frac{1}{\pi}\int_C&\left(\frac{\partial}{\partial u}S_{m_1,j_1,\mathrm{a}}(r,\varphi)\right)\cdot\\&\left(\frac{\partial}{\partial v}S_{m_2,j_2,\mathrm{b}}(r,\varphi)\right),\end{aligned} \tag{20}$$

assuming c/r_p=1. As a consequence of the Eqs. (66) to (71) and the orthonormality of the Zernike polynomials, the second moments are different from zero only if either m_2=m_1 or m_2=m_1–2.

– m_1=m_2
This case also requires j_1=j_2. It describes the effects due to a single slope Zernike polynomial. For m≥2 one obtains:

$$\mu_{xx}=\mu_{yy}=\frac{1}{2}, \tag{21}$$

$$\mu_{xy}=0, \tag{22}$$

and thus ϵ_n=0. Therefore, aberrations expressible by single slope Zernike polynomials with m≥2 and, clearly, also m=0 do not generate ellipticities.

For m=1, with the angle of the symmetry axis of the wavefront with respect to the x-axis of the field denoted by ϑ,

$$\mu_{xx}=\frac{1}{2}+\frac{1}{4}\cos 2\vartheta, \tag{23}$$

$$\mu_{yy}=\frac{1}{2}-\frac{1}{4}\cos 2\vartheta, \tag{24}$$

$$\mu_{xy}=\frac{1}{4}\sin 2\vartheta. \tag{25}$$

Therefore, according to Eqs. (5) and (6),

$$\epsilon_\mathrm{n}=\frac{1}{2},\ \alpha=\vartheta. \tag{26}$$

This result for m=1 is independent of the order j of the slope Zernike polynomial. In other words, all coma-like aberrations with identical coefficients of the slope Zernike polynomials $S_{1,j}(r, \varphi)$ generate the same ellipticities.

– m_2=m_1−2
This case describes ellipticities that are generated by combinations of two slope Zernike polynomials with rotational symmetries differing by 2. The ellipticities are different from zero only if, in addition, j_2=j_1+1. In other words, only combinations of slope Zernike polynomials with m_2=m_1–2 and the same highest radial powers generate ellipticities.

In summary, for c/r_p=1, Table 1 shows the values for the ellipticities $\beta_{m,j,m',j}=\epsilon_n$ for all possible single terms and combinations that can give rise to ellipticities. A square bracket denotes that the value of $\beta_{m,j,m',j'}$ is only due to the combined effect of two terms and not to any of the two individual terms. Ellipticities due to individual terms can only be generated by coma-type slope Zernike polynomials $S_{1,j}(r, \varphi)$, which will only appear in the combinations $\{(3, j), (1, j+1)\}$.

2.3 Characterization of field dependencies by Zernike polynomials

For the understanding of the field dependencies of the spot sizes and ellipticities, it would be helpful to express the field dependencies in terms of simple functions. For a circular field, a convenient set of functions are the Zernike polynomials. These now depend on the normalized radial field variable s and the field azimuth angle ϑ, instead of on the normalized radial aperture variable r and the aperture azimuth angle φ as the Zernike or, as in this study, slope Zernike polynomials used for the aperture dependence of aberrations. This type of expansion has been discussed in [12], using standard Zernike polynomials both for the pupil and the field.

Table 1 Ellipticities generated by single or combinations of slope Zernike polynomials.

Modes	$\beta_{m,j,m',j'}$
$(1, j)$ $j>1$	1/2
$[(2, 1), (0, 2)]$	2
$(2, j), (0, j+1)$ $j>1$	$\sqrt{2}$
$(m, 1), (m-2, 2)$ $m\geq 3$	$\sqrt{2}$
$(m, j), (m-2, j)$ $m\geq 3$ $j>1$	1

In many telescopes, the detector fields are square instead of circular. To guarantee the linear independence of the coefficients of the field dependencies, one should use polynomials that are orthogonal over a square. However, these are not easily classifiable in terms of rotational symmetries and would complicate the expressions considerably. Therefore, in this paper the field dependencies are described in terms of standard circular Zernike polynomials.

If the measured ellipticities were described by the modulus $\sigma_l^2-\sigma_s^2$ and the angle α_m, their field dependencies could not always be easily expanded in terms of Zernike polynomials. As an example, one can take the combination of constant defocus and rotationally symmetric field astigmatism and calculate the dependencies of the generated ellipticities on the radial field coordinate s and the azimuth field coordinate ϑ.

For symmetry reasons, the dependence of the rotationally symmetric astigmatism on the field radius can only contain even powers of s.

The angles of the ellipticities depend, on the one hand, on the angles of the maxima of the astigmatism in the pupil, and, on the other hand, on the sign of the defocus. With a defocus that is constant across the field, the directions of the ellipticities then rotate with ϑ and their x- and y-components are proportional to cos ϑ or sin ϑ, as shown in Figure 1 by the red bars.

Combining the radial and angular dependencies, the expressions contain even powers of s and the functions cos ϑ or sin ϑ with an odd rotational symmetry. Such expressions cannot naturally and easily be expressed by standard Zernike polynomials.

However, this problem can be solved by multiplying the measured angles α_m of the ellipticities by a factor of 2, as already discussed in Section 2.1. Then, the angles of the ellipticities $\vec{\epsilon}$ rotate with 2ϑ, as shown in Figure 1 by the green arrows. The components ϵ_x and ϵ_y of the ellipticity

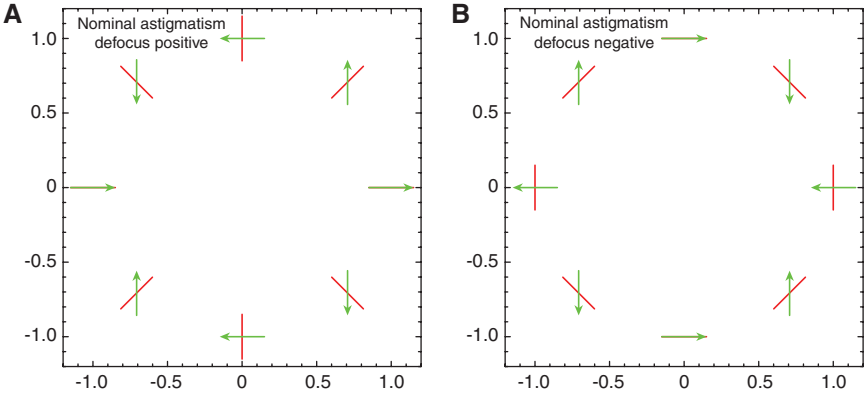

Figure 1 Measured angles of the ellipticities (red) and corresponding angles of the ellipticity vectors $\vec{\epsilon}$ (green) for rotationally symmetric astigmatism in combination with (A) positive and (B) negative constant defocus.

patterns can then be expressed by low-order Zernike polynomials $Z_{2,j}(s, \vartheta)$.

Another example is a misaligned system with linear field astigmatism (see Section 3.3.2), whose modulus is proportional to the radial field coordinate s and whose orientation changes with half the field angle $\vartheta/2$. The ellipticities, generated in combination with a constant defocus, will have the same field dependencies, as shown in Figures 2 and 3 by the red bars. After doubling the angle, the field dependence of the components ϵ_x and ϵ_y of the ellipticities patterns are proportional to $s \cos \vartheta$ and $s \sin \vartheta$, as shown in Figures 2 and 3 by the green arrows. Therefore, they can be expressed by the Zernike polynomials $Z_{1,1}(s, \vartheta)$.

Figures 1–3 also show that a change of the sign of the defocus rotates the measured, true angles of the ellipticities by 90°, whereas the corresponding ellipticity vectors $\vec{\epsilon}$ are converted to $-\vec{\epsilon}$. This is another reason why the ellipticity vectors $\vec{\epsilon}$ are more suitable for relating ellipticities to aberrations than the ellipticities defined with the measured angles.

3 Aberrations affecting ellipticities and spot sizes

3.1 Assumed wavefront error

Any wavefront error anywhere in the field can be expanded in terms of slope Zernike polynomials across the aperture:

$$\begin{aligned} w(r,\varphi,s,\vartheta) &= \sum_{m=0}^{\infty}\sum_{j=1}^{\infty} F_{m,j}(s,\vartheta)[\cos(m\theta_{m,j}(\vartheta))S_{m,j,c}(r,\varphi) \\ &\quad + \sin(m\theta_{m,j}(\vartheta))S_{m,j,s}(r,\varphi)] \\ &= \sum_{m=0}^{\infty}\sum_{j=1}^{\infty}(G_{m,j,c}(s,\vartheta)S_{m,j,c}(r,\varphi) \\ &\quad + G_{m,j,s}(s,\vartheta)S_{m,j,s}(r,\varphi)), \end{aligned} \tag{27}$$

where $\theta_{m,j}(\vartheta)$ is the offset angle of the slope Zernike polynomial expressed as $\tilde{B}_{m,j}\cos m(\varphi - \theta_{m,j}(\vartheta))$. The angle $\theta_{m,j}$ is assumed to depend only on the field angle ϑ and not on

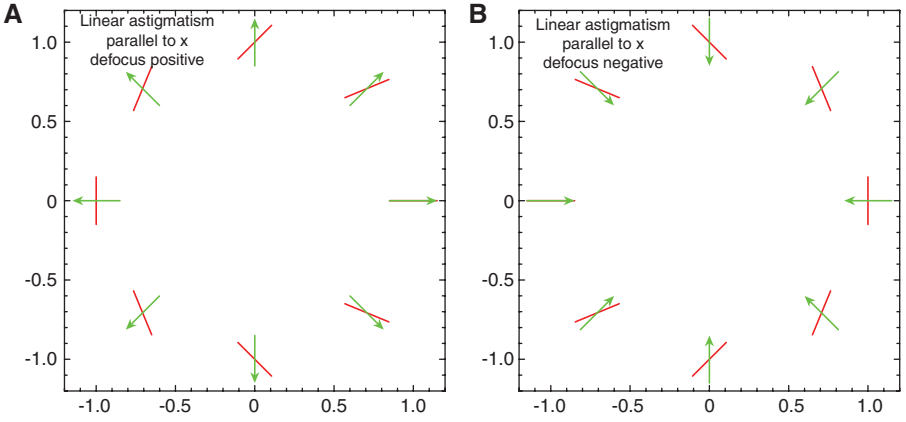

Figure 2 Measured angles of the ellipticities (red) and corresponding angles of the ellipticity vectors $\vec{\epsilon}$ (green) for linear astigmatism along x in combination with (A) positive and (B) negative constant defocus.

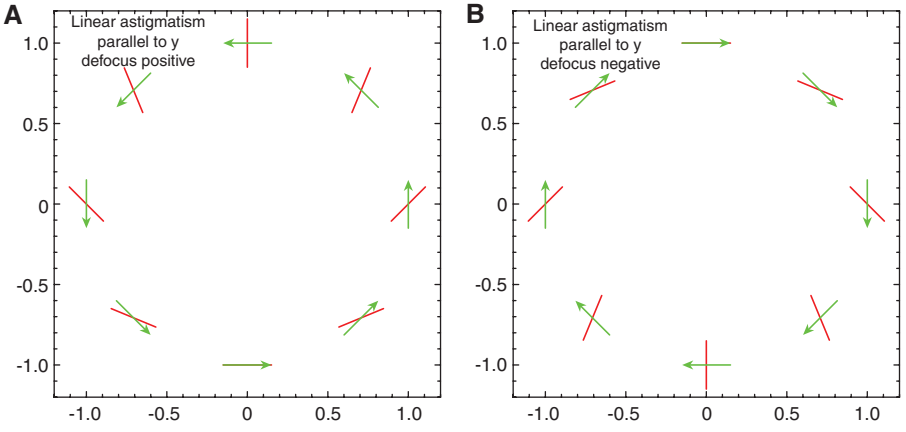

Figure 3 Measured angles of the ellipticities (red) and corresponding angles of the ellipticity vectors $\vec{\epsilon}$ (green) for linear astigmatism along y in combination with (A) positive and (B) negative constant defocus.

the field radius s. $F_{m,j}(s, \vartheta)$ describes the field dependence of $(S_{m,j,c}(r, \varphi)^2+S_{m,j,s}(r, \varphi)^2)^{1/2}$ and the functions $G_{m,j,c}(s, \vartheta)$ and $G_{m,j,s}(s, \vartheta)$ describe the field dependencies of the slope Zernike polynomials $S_{m,j,c}(r, \varphi)$ and $S_{m,j,s}(r, \varphi)$, respectively. Products of pairs of these functions G will appear in the expressions for the spot sizes and the ellipticities.

Because the r and φ dependencies drop out after the integrations leading to the μ_{xx}, μ_{yy} and μ_{xy} terms, the field dependencies of the spot sizes and ellipticities are entirely determined by the field dependencies $F_{m,j}(s, \vartheta)$ of the coefficients of the slope Zernike polynomials and by the symmetry m and the offset angles $\theta_{m,j}(\vartheta)$ in the slope Zernike polynomials. It will be shown that all field dependencies of the spot sizes and ellipticities can, in a simple way, be expanded across the field in Zernike polynomials that depend on the field variables s and ϑ.

3.2 Aberrations of the unperturbed system

Every real optical system contains field aberrations. The system may either be the one defined by its prescription or by the as-built status. In the following, either system, as long as it is rotationally symmetric, will be called the nominal system.

The ESO VLT Survey Telescope (VST) [13], a survey telescope with an outer diameter of 2.6 m, an inner diameter of 1.2 m and a diagonal field diameter of 1.5°, will serve as an example of a wide-field telescope. In addition to two powered mirrors, the VST also contains a three-element lens corrector, which causes a strong dependence of some of the nominal telescope aberrations on the wavelength of the light. This is discussed in more detail in Section 4.8.3. All curves in the figures in this section are based on a wavelength of 625 nm, which is roughly the center of the R-band filter in the VST.

In a telescope perfectly matching its optical prescription, the strongest field aberrations are, naturally, the lowest-order ones. Figure 4 shows the coefficients $c_{z,m,j}(s)$ of the strongest Zernike aberrations $Z_{m,j}(r, \varphi)$ as functions of the radial field coordinate s. Of the remaining coefficients, the largest one is the coefficient of $Z_{3,1}(r, \varphi)$ with a maximum of only approximately 1.5 nm, whereas the coefficients of all other Zernike polynomials are well below 1 nm.

Instead of the coefficients of the Zernike polynomials, the coefficients that express more directly the influence on the spot sizes and ellipticities are the coefficients $c_{s,m,j}(s)$ of the slope Zernike polynomials $S_{m,j}(r, \varphi)$, which are shown in Figure 5.

Because of the rotational symmetry, the dependence of the coefficients $c_{z,m,j}(s)$ and $c_{s,m,j}(s)$ on the field radius can be described by polynomials in s with only even powers if m is even, and odd powers if m is odd. Table 2 shows the highest powers $n_{hp,m,j}$ in the expansions of the nominal radial field dependencies $F_{m,j}(s)=c_{s,m,j}(s)$, which are required to describe the field dependencies with a precision better than 1%.

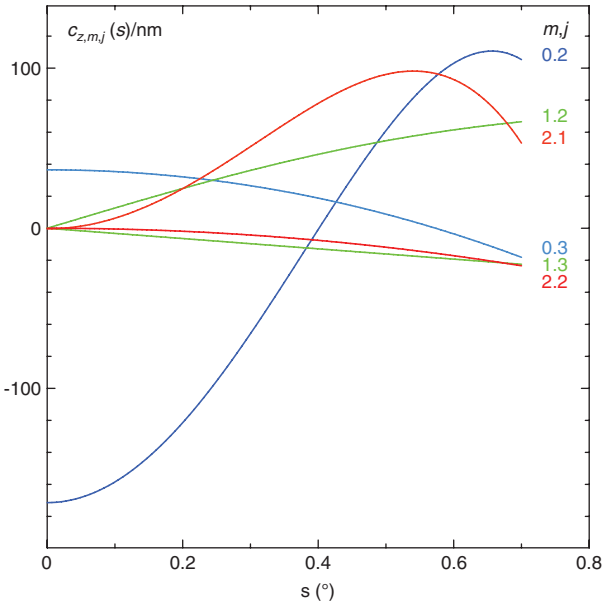

Figure 4 Dependence of the VST coefficients $c_{z,m,j}(s)$ of the Zernike polynomials $Z_{m,j}(r, \varphi)$ on the field radius in degrees.

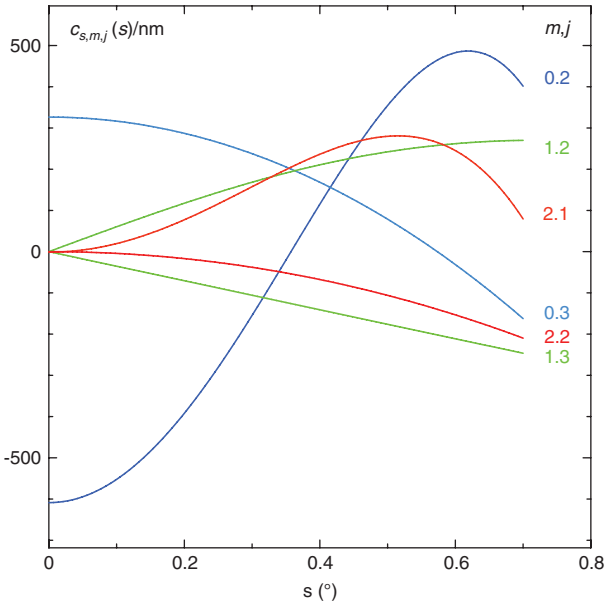

Figure 5 Dependence of the VST coefficients $c_{s,m,j}(s)$ of the slope Zernike polynomials $S_{m,j}(r, \varphi)$ on the field radius in degrees.

Table 2 Highest significant powers of s in the expansions of $c_{s,m,j}(s)$.

(m, j)	(0, 2)	(0, 3)	(1, 2)	(1, 3)	(2, 1)	(2, 2)
$n_{hp,m,j}$	4	2	3	1	4	2

3.3 Telescope errors

3.3.1 Deformations of a mirror

Apart from polishing errors, the most significant aberrations generated by a mirror are low-order aberrations with coefficients that decline rapidly with the order of the mode. If the mirror is at a pupil, all of these aberrations are constant across the field. If the mirror is not at a pupil, the shifts of the footprints in wide-field telescopes are only small fractions of the diameter of the mirror. The field aberrations generated by the deformations of the mirror are then negligible.

The low-order pupil aberration can best be described by elastic modes [14]. However, for the lowest orders the elastic modes are very similar to Zernike polynomials and can, therefore, also be expressed rather accurately by sums of slope Zernike polynomials.

For the low-order coefficients $c_{z,m,j}$ and $c_{s,m,j}$, Table 3 shows the approximate differences between the coefficients measured at the VST pointing to the zenith and close to the horizon, without any corrective actions of the active optics system. The row in the middle shows the conversion factors.

The contributions to the coefficients of defocus $S_{0,2}(r)$ and third-order coma $S_{1,2}(r, \varphi)$ due to a deformation of a mirror cannot be disentangled from the contributions due a misalignment of mirrors. The comparatively large coefficients of defocus $S_{0,2}(r)$ and third-order coma $S_{1,2}(r, \varphi)$ are probably mainly due to misalignments rather than mirror deformations.

Without active optics corrections, third-order coma then generates ellipticities of the order of $200\epsilon_{WL}$ and the combination of third-order astigmatism with defocus ellipticities of approximately $120\epsilon_{WL}$.

3.3.2 Misalignments of telescope mirrors

Misalignments of the telescope primary mirror (M1) or secondary mirror (M2) may be due to axial or lateral movements or tilts, with five degrees of freedom for the misalignment of each mirror. Such misalignments will shift the center of the field, which is defined here as the image formed by rays initially parallel to the M1 axis. In the VST, misalignments of the mirrors within the expected range will lead to shifts of the center of the field in the focal plane that are insignificant compared with the field diameter.

However, misalignments also generate field aberrations. Axial displacements will predominantly generate defocus. The smaller amounts of spherical aberration will be neglected. The other degrees of freedom will generate three types of aberrations.

- *Coma* $S_{1,2}(r, \varphi)$, which is constant across the field.
- *Astigmatism* $S_{2,1}(r, \varphi)$ with a linear radial field dependence, called linear astigmatism:

$$w_{2,1,\mathrm{lin}}(r,\varphi,s,\vartheta)=c_{2,1,\mathrm{lin}}s\tilde{B}_{2,1}(r)\cos 2\left(\varphi-\frac{1}{2}(\vartheta-\vartheta_{2,1})\right), \quad (28)$$

  where the offset angle $\vartheta_{2,1}$ is the field angle, where the line through the maxima of the astigmatism in the pupil is parallel to the field angle.
- *Defocus* $S_{0,2}(r)$ in the focal plane, generated by a tilt of the focal plane. It has a linear field dependence along a direction $\vartheta_{0,2}$ and is expressible as:

$$w_{0,2,\mathrm{lin}}(r,s,\vartheta)=c_{0,2,\mathrm{lin}}s\cos(\vartheta-\vartheta_{0,2})\,S_{0,2}(r). \quad (29)$$

3.3.3 Tilt of the adaptor or detector

Similar to a tilt of the focal plane, a tilt of the adaptor or the detector with respect to the nominal optical axis will introduce defocus with a linear field dependence, as described in Eq. (29).

3.3.4 Tracking

Normal tracking errors will generate spot movements that are constant across the field. An incorrect derotation will generate spot movements in azimuthal direction, which are rotationally symmetric and proportional to the modulus s of the field angle. For typical integration times of 1 min, both tracking errors should be small fractions of 1 arcsec.

Table 3 Variations of the coefficients $c_{z,m,j}$ of the Zernike polynomials and $c_{s,m,j}$ of the slope Zernike polynomials without active optics corrections.

	0, 2	0, 3	1, 2	2, 1	3, 1
$c_{z,m,j}$/nm	500	60	400	200	80
	$2\sqrt{6}$	$4\sqrt{5}$	$4\sqrt{3}$	$2\sqrt{3}$	$2\sqrt{6}$
$c_{s,m,j}$/nm	2500	500	2800	700	400

3.4 Atmospheric dispersion

The field dependence of the atmospheric dispersion can be split into two parts. First, an average component,

which is constant across the field and, second, a component, which varies linearly across the field along the altitude direction. The average part is the dominant one.

4 Field patterns of spot sizes and ellipticities

4.1 Spot sizes and ellipticities in a rotationally symmetric system

4.1.1 Wavefront error

In a rotationally symmetric system, the moduli of the field aberrations are rotationally symmetric and, therefore, independent of ϑ. In addition, $\theta_{m,j}(\vartheta)$ in Eq. (27) is given by $\theta_{m,j}(\vartheta)=\vartheta$. The general wavefront error can then be written as:

$$w(r,\varphi)=\sum_{m=0}^{\infty}\sum_{j=1}^{\infty}F_{m,j}(s)\tilde{B}_{m,j}(r)\cos m(\varphi-\vartheta). \tag{30}$$

where $F_{m,j}(s)$ is a polynomial in s.

4.1.2 Spot sizes

Using Eq. (4) and the orthonormality of the derivatives of the slope Zernike polynomials expressed in Eq. (19), the contributions of the wavefront error to the mean square of the spot size is given by:

$$d_{\text{spot}}^2(s)=\frac{1}{r_{\text{p}}^2}\sum_{m=0}^{\infty}\sum_{j=1}^{\infty}F_{m,j}^2(s) \tag{31}$$

4.1.3 Ellipticities

Ellipticities are generated either by coma $S_{1,j}(r,\varphi)$ alone or by combinations of two terms.

Coma

In the case of coma, with

$$\begin{aligned}w(r,\varphi,s,\vartheta)=\sum_{j=2}^{\infty}F_{1,j}(s)[&\cos\vartheta\, S_{1,j,\text{c}}(r,\varphi)\\&+\sin\vartheta\, S_{1,j,\text{s}}(r,\varphi)],\end{aligned} \tag{32}$$

the quantities ϵ and $\alpha(\vartheta)$ are, using the factor $\beta_{1,j,1,j}=1/2$ from Table 1, given by:

$$\epsilon=\frac{1}{2r_{\text{p}}^2}\sum_{j=2}^{\infty}F_{1,j}(s)^2, \tag{33}$$

$$\alpha=\vartheta. \tag{34}$$

As expected, in a rotationally symmetric system the elongation patterns generated by coma always follow a onefold rotational symmetry. After doubling the angle ϑ, the x- and y-components of the ellipticities are given by:

$$\epsilon_{\text{x}}=\frac{1}{2r_{\text{p}}^2}\sum_{j=2}^{\infty}F_{1,j}^2(s)\cos 2\vartheta, \tag{35}$$

$$\epsilon_{\text{y}}=\frac{1}{2r_{\text{p}}^2}\sum_{j=2}^{\infty}F_{1,j}^2(s)\sin 2\vartheta. \tag{36}$$

Because the rotational symmetry of these expressions is equal to 2 and the powers of s in $F_{1,j}^2(s)$ are even and equal or larger than 2, these expressions can easily be expanded in terms of Zernike polynomials $Z_{2,j}(s,\vartheta)$.

Combinations of two aberrations

In the case of combinations of two terms, one can restrict the calculation of ellipticities to combinations with $m_1=m$, $m_2=m-2$, $j_1=j$, $j_2=j+1$:

$$\begin{aligned}w(r,\varphi)=&F_{m,j}(s)\tilde{B}_{m,j}(r)\cos m(\varphi-\vartheta)\\&+F_{m-2,j+1}(s)\tilde{B}_{m-2,j+1}(r)\\&\cos(m-2)(\varphi-\vartheta).\end{aligned} \tag{37}$$

Using the factors $\beta_{m,j,m-2,j+1}$ defined in Table 1, the quantities ϵ and $\alpha(\vartheta)$ are given by:

$$\epsilon=\frac{1}{r_{\text{p}}^2}\beta_{m,j,m-2,j+1}F_{m,j}(s)F_{m-2,j+1}(s), \tag{38}$$

$$\alpha=\vartheta. \tag{39}$$

Similar to the case of coma, in a rotationally symmetric system the elongation patterns generated by combinations of aberrations always follow a onefold rotational symmetry. After doubling the angle ϑ, the x- and y-components of the ellipticities are given by:

$$\epsilon_{\text{x}}=\frac{1}{r_{\text{p}}^2}\beta_{m,j,m-2,j+1}\,F_{m,j}(s)\,F_{m-2,j+1}(s)\cos 2\vartheta, \tag{40}$$

$$\epsilon_y = \frac{1}{r_p^2}\beta_{m,j,m-2,j+1} F_{m,j}(s)\, F_{m-2,j+1}(s) \sin 2\vartheta. \tag{41}$$

The powers of s in the expansions of $F_{m,j}(s)$ and $F_{m-2,j+1}(s)$ are either both even or both odd. Therefore, the powers in an expansion of the product $F_{m,j}(s)F_{m-2,j+1}(s)$ are all even. Given that, in addition, the rotational symmetries in the expressions in Eqs. (40) and (41) are equal to 2, these expressions can be expanded in terms of Zernike polynomials $Z_{2,j}(s, \vartheta)$.

4.1.4 Nominal ellipticities in the VST

According to Table 2, the maximum significant powers of s are 8 for $F_{2,1}(s)F_{0,2}(s)$, 6 for $F_{1,2}^2(s)$, 4 for $F_{2,2}(s)F_{0,3}(s)$ and 2 for $F_{1,3}^2(s)$. Therefore, a description of the nominal ellipticity pattern in the VST requires the Zernike polynomials $Z_{2,j}(s, \vartheta)$, with j=1, 2, 3, 4.

Figure 6 shows the normalized ellipticities ϵ/ϵ_{WL}, generated by $S_{1,2}(r, \varphi)$, $S_{1,3}(r, \varphi)$ and by the combinations of $S_{2,1}(r, \varphi)$ with $S_{0,2}(r)$ and $S_{2,2}(r, \varphi)$ with $S_{0,3}(r)$. Because the coefficients of the slope Zernike polynomials do not decline as fast with the order of the polynomials as the coefficients of the Zernike polynomials, also the last pair $\{S_{2,2}, S_{0,3}\}$ significantly contributes to the ellipticities.

Figure 6 also demonstrates that the ellipticities generated by the nominal aberrations are well above the weak lensing threshold ϵ_{WL}.

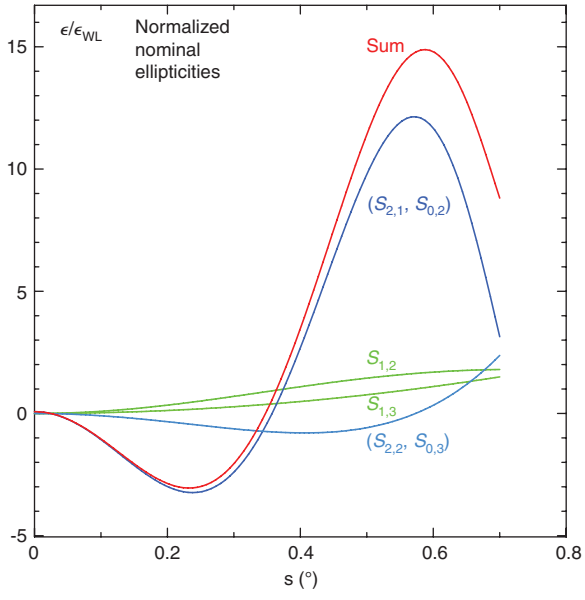

Figure 6 Ellipticities ϵ generated by nominal low-order aberrations and the sum of these ellipticities (red) in an optically perfect VST.

Figure 7 shows the expected rotationally symmetric ellipticity pattern for the optically perfect VST with the true angles α and Figure 8 shows the ellipticity vectors $\vec{\epsilon}$ with the angles 2α. The length of the red horizontal bars at the top of Figures 7 and 8 corresponds to $10\epsilon_{WL}$.

4.2 Spot sizes and ellipticities due to single aberrations

Some low-order aberrations contain terms that are due to more than one error source and have different field dependencies. This section shows that also in this case the field dependencies of the sum of these terms can be expressed by Zernike polynomials.

4.2.1 Defocus

Let $c_{0,2}(s)$ be the field coefficient of the $S_{0,2}(r)$ representing nominal, rotationally symmetric defocus, $c_{0,2,co}$ the coefficient of an $S_{0,2}(r)$ that is constant across the field, and $c_{0,2,lin}$ the coefficient of an $S_{0,2}(r)$ with a linear field dependence as defined in Eq. (29), setting $\vartheta_{0,2}$ = 0. The contribution to the spot size is given by:

$$d^2_{spot,0,2}(s,\vartheta) = \frac{1}{r_p^2}\left(c_{0,2}(s) + c_{0,2,lin}\, s\cos\vartheta + c_{0,2,co}\right)^2 \tag{42}$$

Because $c_{0,2}(s)$ is a polynomial with even powers of s, the field dependence of $d^2_{spot,0,2}$ can be expressed in terms of Zernike polynomials $Z_{0,j}(s)$, $Z_{1,j}(s)$ and $Z_{2,1}(s, \vartheta)$.

4.2.2 Third-order coma

Let $c_{1,2}(s)$ be the field coefficient of $S_{1,2}(r, \varphi)$ representing nominal, rotationally symmetric third-order coma, and $c_{1,2,co,c}$ and $c_{1,2,co,s}$ the coefficients of $S_{1,2,c}(r, \varphi)$ and $S_{1,2,s}(r, \varphi)$, respectively, that are constant across the field. The contribution to the spot size is given by:

$$\begin{aligned} d^2_{spot,1,2}(s,\vartheta) = \frac{1}{r_p^2}\big(&c^2_{1,2}(s) + c^2_{1,2,co,c} + c^2_{1,2,co,s} \\ &+ 2c_{1,2}(s)\left(c_{1,2,co,c}\cos\vartheta + c_{1,2,co,s}\sin\vartheta\right)\big). \end{aligned} \tag{43}$$

Coma alone also generates ellipticities. The contributions to the x- and y-components of the ellipticity $\vec{\epsilon}_{1,2}$ are given by:

$$\begin{aligned} \epsilon_{1,2,x}(s,\vartheta) = \frac{1}{2r_p^2}\big(&c^2_{1,2}(s)\cos 2\vartheta \\ &+ 2c_{1,2}(s)\left(c_{1,2,co,c}\cos\vartheta - c_{1,2,co,s}\sin\vartheta\right) \\ &+ c^2_{1,2,co,c} - c^2_{1,2,co,s}\big) \end{aligned} \tag{44}$$

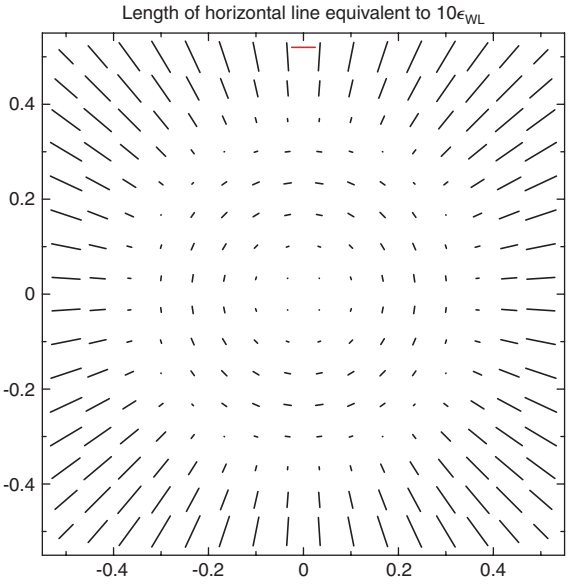

Figure 7 Pattern of the ellipticities ϵ with the true angles α of the perfect VST.

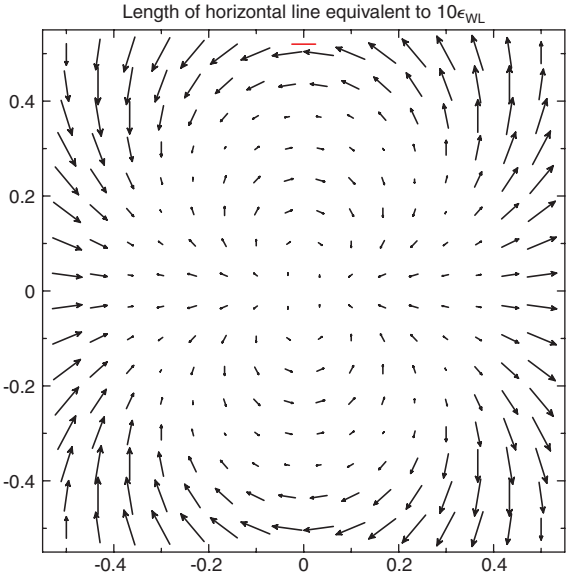

Figure 8 Pattern of the ellipticity vectors $\vec{\epsilon}$ with doubled angles 2α of the perfect VST.

$$\epsilon_{1,2,y}(s,\vartheta)=\frac{1}{2r_p^2}(c_{1,2}^2(s)\sin 2\vartheta +2c_{1,2}(s)(c_{1,2,co,s}\cos\vartheta+c_{1,2,co,c}\sin\vartheta) +2c_{1,2,co,c}c_{1,2,co,s}). \quad (45)$$

Because $c_{1,2}(s)$ is a polynomial with odd powers of s and, therefore, $c_{1,2}^2(s)$ a polynomial with even powers of s, the expression for $d_{\mathrm{spot},1,2}^2(s,\vartheta)$ can be written in terms of Zernike polynomials $Z_{0,j}(s)$ and $Z_{1,j}(s,\vartheta)$ and the ones for $\epsilon_x(s,\vartheta)$ and $\epsilon_y(s,\vartheta)$ in terms of $Z_{0,j}(s,\vartheta)$, $Z_{1,j}(s,\vartheta)$ and $Z_{2,j}(s,\vartheta)$.

4.2.3 Astigmatism

Let $c_{2,1}(s)$ be the field coefficient of the $S_{2,1}(r,\varphi)$ representing nominal, rotationally symmetric third-order astigmatism, $c_{2,1,c}$ and $c_{1,2,s}$ the coefficients of $S_{2,1,c}(r,\varphi)$ and $S_{2,1,s}(r,\varphi)$, respectively, that are constant across the field, and $c_{2,1,\mathrm{lin}}$ the coefficient of linear astigmatism defined in Eq. (28). The contribution to the spot size is given by:

$$\begin{aligned} d_{\mathrm{sp},2,1}^2(s,\vartheta)=\frac{1}{r_p^2}(&c_{2,1}^2(s)+c_{2,1,\mathrm{lin}}^2s^2+c_{2,1,c}^2+c_{2,1,s}^2\\ &+2c_{2,1}(s)\,c_{2,1,\mathrm{lin}}s\cos(\vartheta-\vartheta_{2,1})\\ &+2c_{2,1}(s)\,(c_{2,1,c}\cos 2\vartheta+c_{2,1,s}\sin 2\vartheta)\\ &+2c_{2,1,\mathrm{lin}}\,s\,(c_{2,1,c}\cos(\vartheta-\vartheta_{2,1})\\ &+c_{2,1,s}\sin(\vartheta-\vartheta_{2,1}))). \end{aligned} \quad (46)$$

Because $c_{2,1}(s)$ and therefore also $c_{2,1}^2(s)$ are polynomials with even powers of s, the expression for $d_{\mathrm{spot},1,2}^2(s,\vartheta)$ can be written in terms of Zernike polynomials $Z_{0,j}(s)$, $Z_{1,j}(s,\vartheta)$ and $Z_{2,j}(s,\vartheta)$.

4.3 Tracking and field rotation

Normal tracking errors generate a constant ellipticity, which has to be added vectorially to other ellipticities. A particular tracking error is an incorrect field rotation. With the length of the arc being proportional to the field radius s, the moduli ϵ of the generated ellipticities are proportional to s^2. In addition, after doubling the angle, the orientation changes with 2ϑ. Therefore, the field dependence of the x- and y-dependence of these ellipticities can be expressed by $Z_{2,1}(s,\vartheta)$.

With s=0.7° at the corner of the field, a seeing with an rms of 0.5 arcsec and a field rotation error of φ_{fr}=0.1 arcsec, one would get $\epsilon\approx 20\epsilon_{\mathrm{WL}}$.

4.4 Lateral shift of the field center

A lateral shift of the field center would shift the centers of the contributions due to the rotationally symmetric field errors. It is assumed that the shift is identical for all contributions. If Zernike polynomials are fitted using the shifted field center as the center of the polynomials, the fit should only contain Zernike polynomials that appear in a system where the true field center is in the center of the detector.

The shift of any other aberration can always be expressed by a sum of the aberration and lower-order aberrations, all expressed in terms of slope Zernike polynomials. For example, shifted linear astigmatism can be written as a sum of centered linear astigmatism and constant astigmatism. However, in wide-field telescopes, the shift of the field center is expected to be insignificant compared with the field diameter.

4.5 Atmospheric dispersion

The part of the atmospheric dispersion that is constant across the field generates field-constant ellipticities, whereas the variable part generates ellipticities that can be described by $Z_{1,1}(s, \vartheta)$. Over a wavelength band from 562 nm to 696 nm, typically used in survey telescopes, and at a zenith distance of 45°, the average ellipticity from atmospheric dispersion is of the order of $40\epsilon_{\mathrm{WL}}$, whereas the variation of the ellipticities over a field of 1.5° is only of the order of $2\epsilon_{\mathrm{WL}}$.

4.6 Degeneracies

Degeneracies in the ellipticities $\vec{\epsilon}$ are due to several effects.

- The moduli of the ellipticities are proportional to the squares of the coefficients of aberrations with rotational symmetry 1 and to the products of the coefficients of two different aberrations. Therefore, they remain unchanged under the inversion of the signs of the aberrations.
- Different aberrations and combinations of aberrations can generate the same ellipticities. One example is any coma $S_{1,j}(r, \varphi)$ on the one hand, and a combination of astigmatism $S_{2,1}(r, \varphi)$ and defocus $S_{0,2}(r)$ on the other hand, all of them constant across the field.
- The average part of the atmospheric dispersion can generate constant ellipticities similar to the aberrations in the previous item. The variable part of the atmospheric dispersion can, like several other combinations of telescope aberrations, generate ellipticities with a $Z_{1,1}(s, \vartheta)$ dependence.

Therefore, in a hypothetical perfect optical system without any field aberrations, it would not be possible to unambiguously determine all optical errors due to misalignments and mirror deformations. However, in real systems such as wide-field telescopes, the already existing nominal field aberrations lift at least some of these degeneracies.

For example, for defocus $S_{0,2}(r)$, third-order coma $S_{1,2}(r, \varphi)$ and third-order astigmatism $S_{2,1}(r, \varphi)$, a field-constant term will be added to the nominal term. The modifications of the patterns due to telescope errors will then depend on the nominal field aberration and will, therefore, be different from the merely field-constant ellipticities as in the case without nominal field aberrations.

4.7 Example of an ellipticity pattern due to telescope aberrations

Consider the ellipticity pattern that is generated by a rotationally symmetric third-order astigmatism $S_{2,1}(r, \varphi)$ and a defocus $S_{0,2}(r)$ due to a tilt of the focal plane about the y-axis. The wavefront error is then described by the sum of:

$$\begin{aligned} w_{\mathrm{ast}}(s,\vartheta,r,\varphi) &= F_{2,1}(s)\tilde{B}_{2,1}(r)\cos 2(\varphi-\vartheta) \\ &= F_{2,1}(s)[\cos 2\vartheta\, S_{2,1,\mathrm{c}}(r,\varphi) \\ &\quad +\sin 2\vartheta\, S_{2,1,\mathrm{s}}(r,\varphi)] \end{aligned} \tag{47}$$

and

$$w_{\mathrm{def}}(s,\vartheta,r) = c_{0,2,\mathrm{lin}}\, s\, \cos\vartheta\, S_{0,2}(r). \tag{48}$$

Using Eqs. (3), (5), (6) and (66) to (71) and the factor $\beta_{2,1,0,2}=2$ from Table 1, one obtains for the dependence of ϵ and the true angle α on the field coordinates

$$\epsilon = \frac{2}{r_{\mathrm{p}}^2} c_{0,2,\mathrm{lin}}\, s\, F_{2,1}(s)\cos\vartheta, \tag{49}$$

$$\alpha = \vartheta. \tag{50}$$

The field dependence of ϵ with the true angle α is shown in Figure 9. The angle is only in agreement with Eq. (50) if the sudden rotation of the orientation by 90° on the y-axis of the field is interpreted as a change of the sign in the expression for ϵ. After doubling the angle α, the angle of the vector $\vec{\epsilon}$ changes by 180° along the x-axis, as shown in Figure 10. Again, these considerations justify the definition of the angles in Section 2.1.

The field dependencies of the x- and y-components of $\vec{\epsilon}$ are given by:

$$\epsilon_{\mathrm{x}}(s,\vartheta) = \frac{1}{r_{\mathrm{p}}^2} c_{0,2,\mathrm{lin}}\, s\, F_{2,1}(s)(\cos\vartheta + \cos 3\vartheta) \tag{51}$$

$$\epsilon_{\mathrm{y}}(s,\vartheta) = \frac{1}{r_{\mathrm{p}}^2} c_{0,2,\mathrm{lin}}\, s\, F_{2,1}(s)(\sin\vartheta + \sin 3\vartheta). \tag{52}$$

According to Table 2, for the VST the highest power of s in the polynomials $F_{2,1}(s)$ is 4. Consequently, the

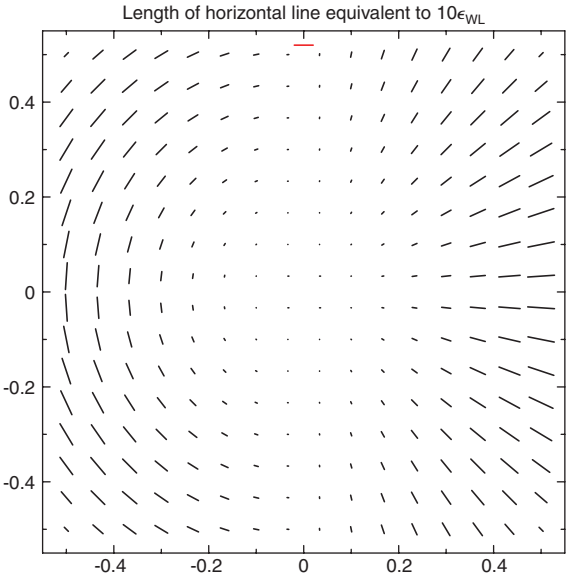

Figure 9 Ellipticities with true angles α generated by defocus $S_{0,2}(r)$, due to a tilt of the focal plane, with $c_{0,2,\mathrm{lin}}$=1000 nm and nominal third-order astigmatism $S_{2,1}(r, \varphi)$ of the VST.

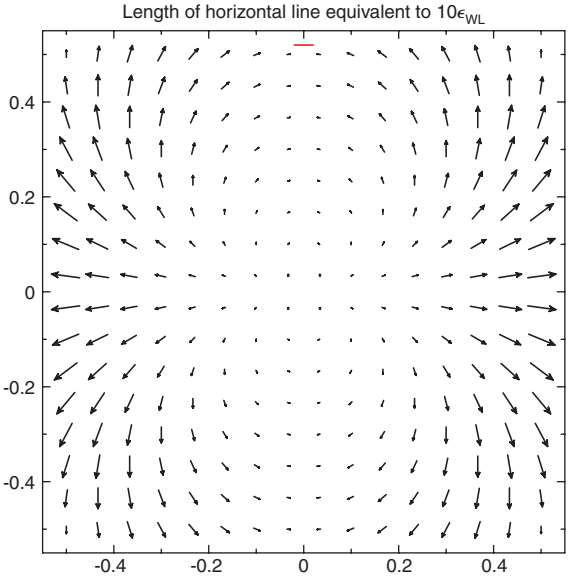

Figure 10 Ellipticities vectors $\vec{\epsilon}$ with angles 2α generated by defocus $S_{0,2}(r)$, due to a tilt of the focal plane, with $c_{0,2,\mathrm{lin}}$=1000 nm and nominal third-order astigmatism $S_{2,1}(r, \varphi)$ of the VST.

dependencies of the expressions in Eqs. (51) and (52) on the field radius s can be expressed as polynomials with odd powers of s and a minimum power of 3 and a maximum power of 5. Therefore, the field dependencies of the x- and y-components of $\vec{\epsilon}$ contain the Zernike polynomials $Z_{1,1}(s, \vartheta)$, $Z_{1,2}(s, \vartheta)$, $Z_{1,3}(s, \vartheta)$, $Z_{3,1}(s, \vartheta)$ and $Z_{3,2}(s, \vartheta)$.

Further examples for ellipticity patterns generated by specific telescope aberrations are given in Appendix 7.4.

4.8 Noise

Three sources of noise will affect the measurement of the effects of telescope errors on the spot sizes and ellipticities. One is the noise in the measurement of the spot sizes and ellipticities of individual spots (shot noise, read-out noise, finite pixel size, etc.), the second one is due to aberrations generated by atmospheric turbulence, and the third one is caused by the dependence of the nominal telescope aberrations on the wavelength of the light.

4.8.1 Photon noise

For a single star the measurement noise is expected to be Gaussian. The ultimate precision with which the ellipticities can be measured is related to the precision with which the rms values of the spot sizes in the direction of the long and short axes can be measured. The precision limit or Cramér-Rao bound can be estimated by calculating the related Fisher information.

Assuming an elliptical Gaussian profile for the spots, the probability distribution for the intensities of a spot centered at the origin is given by:

$$p(x, y, \sigma_x, \sigma_y) = \frac{1}{2\pi\sigma_x\sigma_y} \exp\left(-\frac{x^2}{2\sigma_x^2} - \frac{y^2}{2\sigma_y^2}\right). \tag{53}$$

The integral over the x-y-plane is equal to 1, which corresponds to the case of a single photon. The Fisher information for σ_x can be defined as:

$$I_F = \int_{-\infty}^{+\infty} dx \int_{-\infty}^{+\infty} dy \frac{1}{p(x, y, \sigma_x, \sigma_y)} \left(\frac{\partial p(x, y, \sigma_x, \sigma_y)}{\partial \sigma_x}\right)^2. \tag{54}$$

The ultimate measuring precision of the mean square of the spot in x-direction is then given by:

$$\sigma_{\sigma_x}^2 = \frac{1}{I_F}. \tag{55}$$

Introducing Eq. (53) into Eqs. (54) and (55) one obtains for one photon:

$$\sigma_{\sigma_x} = \sigma_x. \tag{56}$$

Therefore, the ultimate precision for the measurement of the second moments of a spot is the same as for the measurement of its centroid. With an expected number of approximately 10^4 photo electrons per spot, the ultimate precision limit for measuring the rms of the spot size in

any direction is of the order of $0.01\sigma_x$. Therefore, the errors in the measurement of the ellipticities ϵ are of the order of $\sqrt{2}\cdot 10^{-4}\sigma^2_{\text{seeing}}$, which, according to Eq. (11), is equivalent to $\eta \approx 7\cdot 10^{-5}$. This noise can be reduced by averaging over several stars in a given subfield.

4.8.2 Atmospheric noise

Atmospheric turbulence generates wavefront aberrations, especially in the low-order modes. For very short exposures the aberrations are decorrelated already for field angles of a few arcseconds. For longer exposure times, the isoplanatic angles increase. Because they decrease with the order of the modes, the correlation of the coefficients of the modes across the field will also decrease with the order of the modes.

The effect of the atmosphere can possibly be measured by comparing the patterns of the spot sizes and ellipticities taken in close succession with similar inclinations of the telescope tube. In telescopes such as the ESO VLT, even for exposure times of the order of 30 s, the noise due to the atmosphere is significantly larger than the noise due to the centroiding of the Shack-Hartmann spots [14]. The same may be the case here, that is, the atmospheric noise may be larger than the noise due to the measurements of the second moments. As a consequence, if the patterns of spot sizes and ellipticities across the field are expanded in Zernike polynomials, the coefficients of the polynomials should decrease in a characteristic way with the order of the polynomials.

As measured at the VLT [14], under average seeing conditions of $\sigma_{\text{seeing}} \approx 0.5$ arcsec and integration times of approximately 30 s, the coefficients of $Z_{0,2}(r)$, $Z_{1,2}(r, \varphi)$ and $Z_{2,1}(r, \varphi)$ vary by approximately 120 nm, 85 nm and 140 nm rms, respectively. Scaled down to the diameter of the VST, the coefficients of $S_{0,2}(r)$, $S_{1,2}(r, \varphi)$ and $S_{2,1}(r, \varphi)$ all vary by approximately 200 nm rms. Then, $S_{1,2}(r, \varphi)$ would generate ellipticities of approximately ϵ_{WL} and the combination of $S_{2,1}(r, \varphi)$ with $S_{0,2}(r)$ ellipticities of approximately $3\epsilon_{\text{WL}}$.

4.8.3 Errors due to the dependence of aberrations on wavelength

For the VST, Figure 11 shows the strong dependence of the radial field dependence of the coefficient $c_{s,2,1}(s)$ of third-order astigmatism $S_{2,1}(r, \varphi)$ on the wavelength over a range of 354 nm–880 nm. This strong wavelength dependence

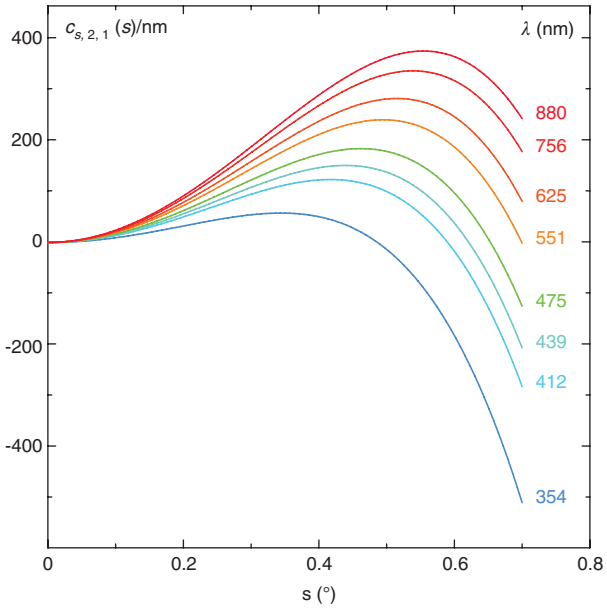

Figure 11 Dependence of the coefficient of $S_{2,1}(r, \varphi)$ of third-order astigmatism on the radial field coordinate s in degrees and on the wavelength λ of the light.

also occurs for the coefficients $c_{s,2,1}(s)$ of defocus $S_{0,2}(r)$ and $c_{s,1,2}(s)$ of third-order coma $S_{1,2}(r, \varphi)$.

Consequently, a random distribution of the star colors would considerably increase the noise in the spot size and ellipticity measurements.

However, in wide-field telescopes, exposures are usually taken with filters like the R-band filter in the VST with bandwidth of the order of 130 nm, for which the variations of the coefficients with wavelength are more constrained.

Nevertheless, Figure 12 shows that, towards the corners of the field, even over such ranges the nominal ellipticities can vary by $10\epsilon_{\text{WL}}$.

4.9 Comparison with Shack-Hartmann measurements

A comparison with the precision of a Shack-Hartmann measurement will be done under the following assumptions.

- The method introduced here uses n_{sf} subfields with one star in each subaperture.
- All stars deliver the same number n_{ph} of photons.
- The only noise is the photon noise.
- The only aberrations are a constant defocus and the ones generated by the atmosphere.
- For one photon, the rms of the centroiding error in the x-direction is then given by $\sigma_{\text{seeing}}/\sqrt{2}$.

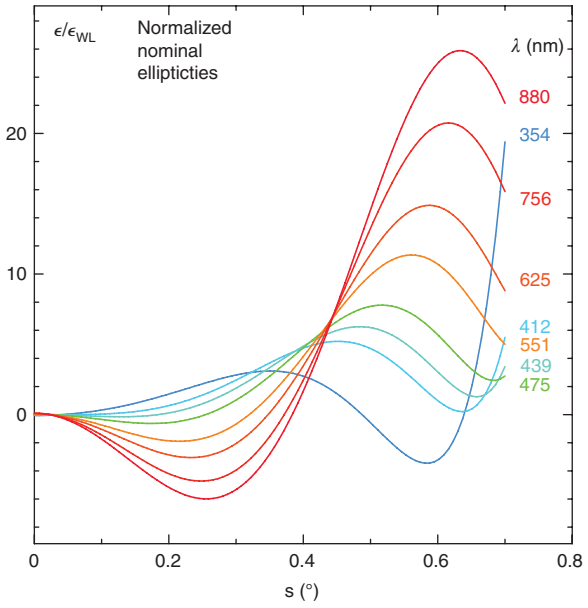

Figure 12 Dependence of the total normalized nominal ellipticity on the radial field coordinate s in degrees and on the wavelength λ of the light.

On the one hand, in the case of the Shack-Hartmann measurement, the rms $\sigma_{0,2,sz}$ of the error of the measurement of the coefficient of defocus $S_{0,2}(r)$ is given by:

$$\sigma_{0,2,sh} = \frac{r_p}{\sqrt{2\,n_{ph}}} \frac{\sigma_{seeing}}{\sqrt{2}} = \frac{r_p}{2\sqrt{n_{ph}}} \sigma_{seeing} \tag{57}$$

This result is independent of the number of subapertures.

On the other hand, the rms σ_{sz} of the spot size derived from measurements of second moments is given by:

$$\sigma_{sz} = \sqrt{\sigma^2_{seeing} + \left(\frac{\sqrt{2}\,c_{0,2}}{r_p}\right)^2} \approx \sigma_{seeing}\left[1 + \frac{1}{2}\left(\frac{\sqrt{2}\,c_{0,2}}{r_p \sigma_{seeing}}\right)^2\right] \tag{58}$$

Regarding σ_{seeing} as a fixed parameter, one obtains for the rms of the variations on both sides of the equation:

$$\sigma_{\sigma_{sz}} = \left(\frac{\sigma_{c_{0,2}}}{r_p \sigma_{seeing}}\right)^2 \sigma_{seeing}. \tag{59}$$

Finally, setting $\sigma_{\sigma_{sz}} = \sigma_{seeing}$ from Eq. (56), one obtains for the rms $\sigma_{0,2,sz}$ of the coefficient of defocus from measurements of the spot size with n_{ph} photons:

$$\sigma_{0,2,sz} = \frac{r_p}{\sqrt{n_{ph}}} \sigma_{seeing} \tag{60}$$

A comparison with Eq. (57) shows that the precision of the measurement of the coefficient of defocus from the size of the spot of one star is approximately the same as the one from a Shack-Hartmann measurement. With n_{sf} subfields the precision limit is given by:

$$\sigma_{0,2,sz} = \frac{r_p}{\sqrt{n_{sf}\,n_{ph}}} \sigma_{seeing}. \tag{61}$$

It is, therefore, much lower than the precision limit for a Shack-Hartmann measurement with a single star.

Similar considerations apply for the use of ellipticities to measure, for example, the precision of the product of the coefficients of defocus $S_{0,2}(r)$ and third-order astigmatism $S_{2,1}(r, \varphi)$.

5 Processing of the ellipticity data

5.1 Elimination of outliers and averaging across subfields

First, the data are filtered by eliminating spots that are too dim or too bright or yield measured values of the spot sizes and of the moduli of the ellipticities $\vec{\epsilon}$ outside reasonable ranges.

Then, the field is divided into typically 16 by 16 subfields. Within each subfield the extreme data are eliminated by a median filter and the remaining data are averaged over the subfields. Figure 13 shows such a pattern of ellipticities $\vec{\epsilon}$ based on a 30-s exposure with the VST after an active optics correction under average seeing conditions [15]. Obviously, the pattern is different from the one of the perfect system shown in Figure 8. Hence, aberrations have a strong impact on the patterns and should be deducible from the patterns.

5.2 Fitting of telescope errors to spot sizes and ellipticities

The averaged ellipticities are further processed by a fitting program. A straightforward, direct approach would be to fit the nominal telescope parameters and the telescope errors to the spot sizes and ellipticities, as shown by the path on the left hand side of Figure 14. The major problem is that the spot sizes and ellipticities depend in a nonlinear way on the wavefront aberrations generated by the telescope. Therefore, the fit requires some kind of trial and error procedure, which may yield solutions that do not correspond to the global minimum.

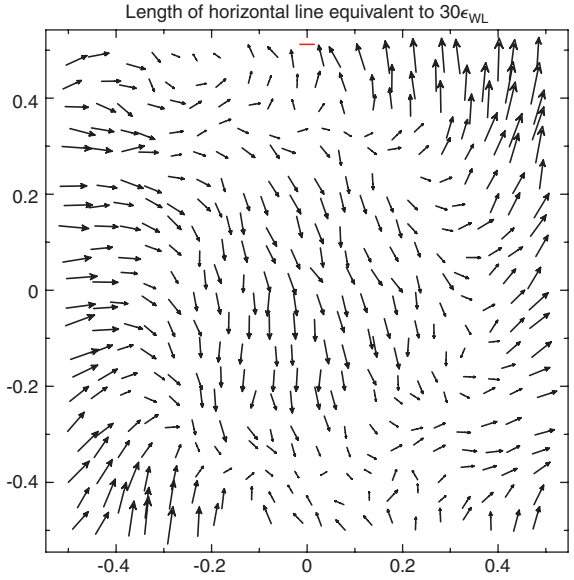

Figure 13 Smoothed and averaged ellipticities $\bar{\epsilon}$ with doubled angles, measured at the VST.

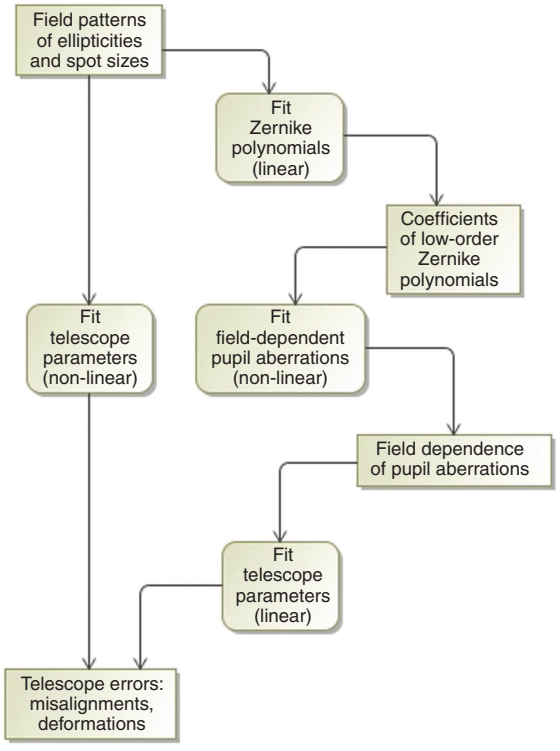

Figure 14 Procedures for fitting telescope errors to field patterns of ellipticities and spot sizes.

5.3 Fitting of Zernike polynomials, telescope aberrations and telescope errors

To gain more insight into the dependencies between the spot sizes and the ellipticities on the one hand and telescope errors on the other hand, one may break up the fitting procedure into three steps, as shown by the path on the right hand side of Figure 14.

1. Zernike polynomials are fitted to the field dependencies of the spot sizes and ellipticities, which is a linear process. Figure 15 shows the fitted pattern of ellipticities using the Zernike polynomials $Z_{0,1}$, $Z_{0,2}$, $Z_{0,3}$, $Z_{1,1}$, $Z_{1,2}$, $Z_{1,3}$, $Z_{2,1}$, $Z_{2,2}$, $Z_{2,3}$, $Z_{2,4}$, $Z_{3,1}$ and $Z_{3,2}$; all of them functions of s and ϑ. Collecting the Zernike polynomials derived in Section 4 and Appendix 7.4, this is the full set of Zernike polynomials in the field patterns of the spot sizes and ellipticities that can be generated by telescope aberrations.
   The fitted pattern looks very similar to the pattern in Figure 13. Figure 16 shows the residual ellipticities, which do not exhibit any regular features. The residual noise is of the order of $7\epsilon_{WL}$, which is of the same order of magnitude as the noise estimated in Sections 4.8.2 and 4.8.3.
2. Pupil aberrations with specific field dependencies, which are generated by the perfect telescope and by telescope errors, are fitted to the coefficients of the Zernike polynomials. As discussed in Section 3, for a telescope such as the VST these would be nominal defocus, third-order coma and third-order astigmatism, field-constant defocus, third-order coma, third-order astigmatism and trefoil, and linear defocus and astigmatism, defined in Eqs. (28) and (29), respectively. In addition, one has to take into account tracking errors and the largely known contributions from atmospheric dispersion.

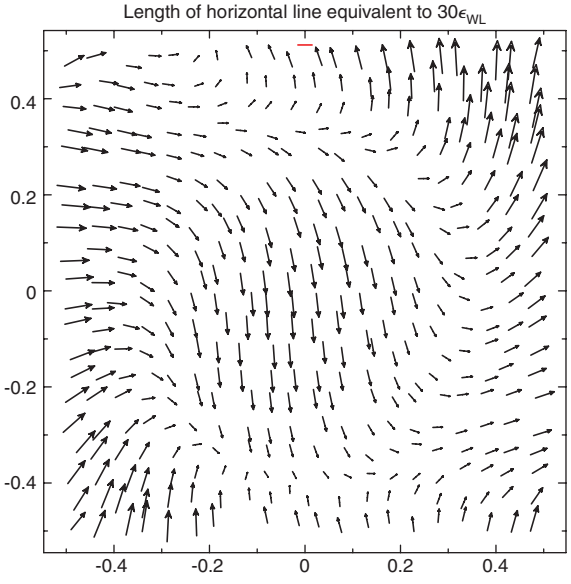

Figure 15 Ellipticities $\bar{\epsilon}$ described as a sum of 12 Zernike polynomials fitted to the measured pattern shown in Figure 13.

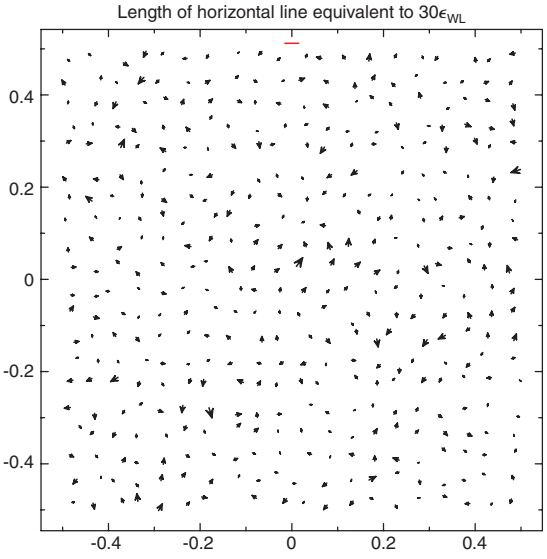

Figure 16 Residual ellipticities $\bar{\epsilon}$ after subtracting a sum of 12 Zernike polynomials fitted to the measured pattern shown in Figure 13.

The relationships between the aberrations and the Zernike polynomials, discussed in Section 4, show that this is a non-linear fit, where degeneracies are not easily identified and which may run into false minima.

3. The telescope errors are fitted to the field aberrations. For the VST, the telescope errors would be the ones discussed in Section 3.3, which are misalignments and mirror deformations. This fit is, similar to the first one, a linear fit (projection), where degeneracies can be detected by singular value decomposition.

A similar analysis can be done for the patterns of the spot sizes. Because the telescope errors can only generate field dependencies with a maximum rotational symmetry of 2, only the first 10 of the 12 Zernike polynomials mentioned under point 1 above need to be fitted to the patterns of the spot sizes.

Because of the degeneracies mentioned above, the non-linear fit may lead to different solutions, which, nevertheless, all lead to similar residual errors. Additional information, as for example from sensors at the edge of the field, may be useful for disentangling the errors and finding the true solutions. The application of the method introduced here to control the image quality of the VST will be presented in a forthcoming paper.

6 Conclusions

Telescope aberrations generate variations in the spot size and in the ellipticities across the field that are often significantly larger than the ones due to centroiding or atmospheric noise. Using a large number of stars across the field, all of these patterns can be accurately described in terms of Zernike polynomials depending on field coordinates. The residual ellipticities after fitting a few low-order Zernike polynomials are of the order of the expected noise. The telescope errors can be deduced from a fit of telescope parameters to either the spot size and ellipticity patterns directly or to the coefficient of the best-fit Zernike polynomials describing the field pattern.

The removal of all features in the patterns that are generated by telescope aberrations should simplify the task of detecting systematic patterns that are generated by other sources.

7 Appendix

7.1 Notations used for Zernike polynomials $Z_{m,j}$ and slope Zernike polynomials $S_{m,j}$

Table 4 Correspondence between indices m, j, the Noll notation and commonly used names for Zernike polynomials.

m	j	Noll notation	Name
0	1	Z_1	Piston
0	2	Z_4	Defocus
0	3	Z_{11}	Spherical aberration
1	1	Z_2, Z_3	Tilt
2	2	Z_7, Z_8	Third-order coma
3	3	Z_{16}, Z_{17}	Fifth-order coma
2	1	Z_5, Z_6	Third-order astigmatism
2	2	Z_{12}, Z_{13}	Fifth-order astigmatism
3	1	Z_9, Z_{10}	Trefoil

7.2 Relationships between normalized and non-normalized Zernike and slope Zernike polynomials

If modified radial components $R_{m,j}(r)$ and $B_{m,j}(r)$ are defined by:

$$R_{m,j}(r)=\begin{cases}\dfrac{1}{\sqrt{2j-1}}\tilde{R}_{0,j}(r) & m=0,\\ \dfrac{1}{\sqrt{2(m+2j-1)}}\tilde{R}_{m,j}(r) & m\geq 1,\end{cases} \tag{62}$$

$$B_{m,j}(r)=\begin{cases}2\sqrt{2(j-1)}\,\tilde{B}_{0,j}(r) & m=0,\\ \sqrt{m}\,\tilde{B}_{m,1}(r) & m\geq 1,\ j=1,\\ \sqrt{2(m+2(j-1))}\,\tilde{B}_{m,j}(r) & m\geq 1,\ j\geq 2,\end{cases} \tag{63}$$

the relationships between Zernike and slope Zernike polynomials are given by:

$$R_{m,j}(r)=\sum_{i=1}^{j} B_{m,i} \tag{64}$$

$$B_{m,j}(r)=R_{m,j}(r)-R_{m,j-1}(r). \tag{65}$$

With $n=m+2(j-1)$, the functions $R_{m,j}(r)$ and $B_{m,j}(r)$ are identical to the functions $R_n^m(r)$ and $B_m^n(r)$ in [11].

7.3 Expression of the derivatives of slope Zernike polynomials in terms of Zernike polynomials

The derivative of a slope Zernike polynomial $S_{m,j,\mathrm{a}}(r,\varphi)$ with respect to x and y can be expressed as a single Zernike polynomial $Z_{1,j,\mathrm{a}}(r,\varphi)$ for $m=0$ or as a sum of two Zernike polynomials $Z_{m,j,\mathrm{b}}(r,\varphi)$ and $Z_{m+1,j-1,\mathrm{b}}(r,\varphi)$ for $m>0$, with a, b$\in$ {c, s}.

$$\frac{\partial}{\partial x}S_{0,j}(r)=+a_{0,j}Z_{1,j-1,\mathrm{c}}(r,\varphi), \tag{66}$$

$$\frac{\partial}{\partial y}S_{0,j}(r)=+a_{0,j}Z_{1,j-1,\mathrm{s}}(r,\varphi) \tag{67}$$

$$\frac{\partial}{\partial x}S_{m,j,\mathrm{c}}(r,\varphi)=+a_{m,j}Z_{m+1,j-1,\mathrm{c}}(r,\varphi)+b_{m,j}Z_{m-1,j,\mathrm{c}}(r,\varphi), \tag{68}$$

$$\frac{\partial}{\partial y}S_{m,j,\mathrm{c}}(r,\varphi)=+a_{m,j}Z_{m+1,j-1,\mathrm{s}}(r,\varphi)-b_{m,j}Z_{m-1,j,\mathrm{s}}(r,\varphi), \tag{69}$$

$$\frac{\partial}{\partial x}S_{m,j,\mathrm{s}}(r,\varphi)=+a_{m,j}Z_{m+1,j-1,\mathrm{s}}(r,\varphi)+b_{m,j}Z_{m-1,j,\mathrm{s}}(r,\varphi), \tag{70}$$

$$\frac{\partial}{\partial y}S_{m,j,\mathrm{s}}(r,\varphi)=-a_{m,j}Z_{m+1,j-1,\mathrm{c}}(r,\varphi)+b_{m,j}Z_{m-1,j,\mathrm{c}}(r,\varphi). \tag{71}$$

The values for the coefficients $a_{m,j}$ and $b_{m,j}$ are shown in Table 5.

Table 5 Coefficients used in Eqs. (66) to (71).

m	c, s	j	$\partial/\partial x$, $\partial/\partial y$	$a_{m,j}$	$b_{m,j}$
0	c, s	>1	$\partial/\partial x$, $\partial/\partial y$	$1/\sqrt{2}$	0
1	c	1	$\partial/\partial x$	0	1
		1	$\partial/\partial y$	0	0
		>1	$\partial/\partial x$	1/2	$1/\sqrt{2}$
		>1	$\partial/\partial x$	1/2	0
1	s	1	$\partial/\partial x$	0	0
		1	$\partial/\partial y$	0	1
		>1	$\partial/\partial x$	1/2	0
		>1	$\partial/\partial y$	1/2	$1/\sqrt{2}$
>1	c, s	1	$\partial/\partial x$, $\partial/\partial y$	0	$1/\sqrt{2}$
		>1	$\partial/\partial x$, $\partial/\partial y$	1/2	1/2

7.4 Examples of ellipticity patterns due to telescope aberrations

7.4.1 Linear astigmatism and defocus due to tilt of focal plane

A linear astigmatism that is symmetric to the x-axis and a linear defocus generated by a tilt of the focal plane around the y-axis are described by:

$$\begin{aligned} w_{\mathrm{ast}} &= c_{2,1,\mathrm{lin}}\, s\, \tilde{B}_{2,1}(r)\cos 2(\varphi-\vartheta/2) \\ &= c_{2,1,\mathrm{lin}}\, s\,[\cos\vartheta\, S_{2,1,\mathrm{c}}(r,\varphi)+\sin\vartheta\, S_{2,1,\mathrm{s}}(r,\varphi),] \end{aligned} \tag{72}$$

and by Eq. (29) with $\vartheta_{0,2}=0$, respectively. Similarly to Section 4.7 one obtains the following expressions:

$$\epsilon=\frac{2}{r_{\mathrm{p}}^2}\, c_{0,2,\mathrm{lin}}\, c_{2,1,\mathrm{lin}}\, s^2\cos\vartheta, \tag{73}$$

$$\alpha=\frac{\vartheta}{2}, \tag{74}$$

$$\epsilon_{\mathrm{x}}=\frac{1}{r_{\mathrm{p}}^2}\, c_{0,2,\mathrm{lin}}\, c_{2,1,\mathrm{lin}}\, s^2\,(1+\cos 2\vartheta), \tag{75}$$

$$\epsilon_{\mathrm{y}}=\frac{1}{r_{\mathrm{p}}^2}\, c_{0,2,\mathrm{lin}}\, c_{2,1,\mathrm{lin}}\, s^2\sin 2\vartheta. \tag{76}$$

Because the dependence on the radial field variable s is proportional to s^2, the field dependencies can be expressed in terms of Zernike polynomials $Z_{0,1,\mathrm{c}}(s)$, $Z_{0,2,\mathrm{c}}(s)$ and $Z_{2,1,\mathrm{c}}(s,\vartheta)$ for ϵ_{x} and $Z_{2,1,\mathrm{s}}(s,\vartheta)$ for ϵ_{y}.

7.4.2 Linear astigmatism and nominal defocus

A linear astigmatism that is symmetric to the x-axis is described in Eq. (72) and a rotationally symmetric nominal defocus by:

$$w_{0,2}(s,\vartheta,r)=F_{0,2}(s)\, S_{0,2}(r). \tag{77}$$

Then,

$$\epsilon=\frac{2}{r_{\mathrm{p}}^2} c_{2,1,\mathrm{lin}}\, s F_{0,2}(s), \tag{78}$$

$$\alpha=\frac{\vartheta}{2}, \tag{79}$$

$$\epsilon_{\mathrm{x}}=\frac{1}{r_{\mathrm{p}}^2} c_{2,1,\mathrm{lin}}\, s F_{0,2}(s)\cos\vartheta, \tag{80}$$

$$\epsilon_y = \frac{1}{r_p^2} c_{2,1,\mathrm{lin}} s F_{0,2}(s) \sin\vartheta. \quad (81)$$

The dependencies of the expressions on the field radius s can be expressed as polynomials with odd powers of s. Therefore, the field dependencies of the x- and y-components of $\vec{\epsilon}$ contain the Zernike polynomials $Z_{1,j}(s, \vartheta)$ with $j \geq 1$.

7.4.3 Trefoil and coma

In the VST, nominal trefoil is negligible. However, the coefficient $c_{3,1,c}$ of field-constant $S_{3,1,c}(r, \varphi)$ in the VST may be of the order of 300 nm. Together with nominal third-order coma $S_{1,2}(r, \varphi)$, it may generate ellipticities of the order of $8\epsilon_{WL}$ with the field dependencies:

$$\epsilon = \frac{\sqrt{2}}{r_p^2} c_{3,1,c} F_{1,2}(s), \quad (82)$$

$$\alpha = \frac{\vartheta}{2}, \quad (83)$$

$$\epsilon_x = \frac{\sqrt{2}}{r_p^2} c_{3,1,c} F_{1,2}(s) \cos\vartheta, \quad (84)$$

$$\epsilon_y = \frac{\sqrt{2}}{r_p^2} c_{3,1,c} F_{1,2}(s) \sin\vartheta. \quad (85)$$

Because $F_{1,2}(s)$ is a polynomial in s with only odd powers, ϵ_x can be expressed by Zernike polynomials $Z_{1,j,c}(s, \vartheta)$ and ϵ_y by Zernike polynomials $Z_{1,j,s}(s, \vartheta)$.

References

[1] M. Liang, V. Krabbendam, C. F. Claver, S. Chandrasekharan and B. Xin, Proc. SPIE 8444, Q8444Q-1-13 (2012).
[2] M. Jarvis and B. Jain, arXiv:astro-ph/0412234 (2004).
[3] M. Jarvis, P. Schechter and B. Jain, arXiv:astro-ph/0810.0027 (2008).
[4] Z. Ma, G. Bernstein, A. Weinstein and M. Sholl, Publ. Astron. Soc. Pac., 120, 1307–1317 (2008).
[5] L. B. Moore, A. M. Hvisc and J. Sasian, Opt. Exp. 20, 15655–15670 (2008).
[6] A. Manuel and J. Burge, Proc. SPIE 7433, 7433A (2009).
[7] P. Schechter and R. Levinson, PASP 123, 812 (2011).
[8] K. Thompson, Adv. Opt. Techn. 2, 89–95 (2013).
[9] C. A. Laury-Micoulout, A&A 51, 343 (1976).
[10] W. Lukosz, Opt. Acta 10, 1–19 (1963).
[11] J. Braat, J. Opt. Soc. Am. 4, 643–650 (1987).
[12] I. W. Kwee and J. J. M. Braat, Pure Appl. Opt. 2, 21–32 (1993).
[13] P. Schipani, M. Capaccioli, C. Arcidiacono, J. Argomedo, M. Dall'Ora, et al., Proc. SPIE 8444, 84441C (2012).
[14] L. Noethe, Prog. Opt. 43, 1–69 (2002).
[15] P. Schipani, L. Noethe, C. Arcidiacono, J. Argomedo, M. Dall'Ora, et al., J. Opt. Soc. Am. A29, 1359 (2012).